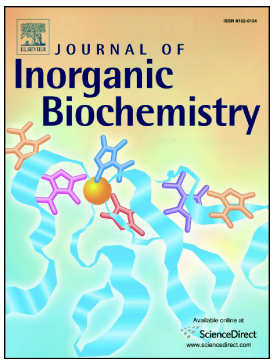

Synthesis, structure, and biological activity of bis(benzimidazole)amino thio- and selenoether nickel complexes

Natalia Muñoz-Patiño, Brenda N. Sánchez-Eguía, Daniela Araiza-Olivera, Marcos Flores-Alamo, Simón Hernández-Ortega, Diego Martínez-Otero, Ivan Castillo

PII: S0162-0134(20)30226-9

DOI: https://doi.org/10.1016/j.jinorgbio.2020.111198

Reference: JIB 111198

To appear in: *Journal of Inorganic Biochemistry*

Received date: 10 June 2020

Revised date: 25 June 2020

Accepted date: 13 July 2020

Please cite this article as: N. Muñoz-Patiño, B.N. Sánchez-Eguía, D. Araiza-Olivera, et al., Synthesis, structure, and biological activity of bis(benzimidazole)amino thio- and selenoether nickel complexes, *Journal of Inorganic Biochemistry* (2020), https://doi.org/10.1016/j.jinorgbio.2020.111198

Synthesis, structure, and biological activity of bis(benzimidazole)amino thio- and selenoether nickel complexes

*Natalia Muñoz-Patiño,[a] Brenda N. Sánchez-Eguía,[a] Daniela Araiza-Olivera,[a] Marcos Flores-Alamo,[b] Simón Hernández-Ortega,[a] Diego Martínez-Otero,[c] and Ivan Castillo[a]**

[a] Instituto de Química, Universidad Nacional Autónoma de México, Circuito Exterior, CU, 04510, México

[b] Facultad de Química, División de Estudios de Posgrado, Universidad Nacional Autónoma de México, Circuito Exterior, CU, 04510, México

[c] Centro Conjunto de Investigación en Química Sustentable, UAEM-UNAM, 50200, Toluca, Estado de México, México.

* Corresponding author. E-mail address: joseivan@unam.mx (I. Castillo).

Abstract

Four new nickel (II) complexes with bis(benzimidazole)thio- and selenoether-based ligands have been synthesized and characterized in the solid state by elemental analysis, IR, magnetic susceptibility and X-ray crystallography, and in solution by FAB^+ mass spectrometry, UV-vis spectroscopy and cyclic voltammetry. Single-crystal X-ray diffraction analysis of the compounds revealed octahedral geometries for all nickel centers. Three of the four complexes are dimers with chloride bridges between the two Ni(II) ions. However, in solution all complexes have a monomeric formulation, based on mass spectrometry and osmometry measurements. The complexes were also screened for their cytotoxic activity on human cell lines (HeLa, SK-LU-1 and HEK-293), and compared with a related Cu(II) complex.

Keywords: Nickel, benzimidazole, X-ray structure, thioether, selenoether, cytotoxicity

1. Introduction

Imidazole derivatives are an important class of nitrogen heterocycles, being the core fragment of different natural products and biological systems. The imidazole ring is biologically relevant as it can mimic the corresponding moiety in histidine. It is able to act as a ligand towards metal ions, potentially enabling them to bind with biomolecules [1]. Benzimidazoles contain a phenyl ring fused to the imidazole, and are of great interest due to their potential applications in several biological areas [2], such as anti-inflammatory [3], antiviral [4], antibacterial [5,6], antifungal [7], antioxidant [8] and antiproliferative/anticancer activities [9–12]. In addition to these properties, bis(benzimidazole) derivatives have attracted great attention because they have a remarkable coordination ability. The derivatives containing two benzimidazole and one central amine, pyridine or other units, act as tridentate ligands for transition metals, and have been employed for modeling biological systems [13,14].

On the other hand, thioethers have recently been reevaluated as important ligands due to their involvement in several chemical and biological systems [15]. Moreover, their redox non-innocent nature as ligands in transition metal complexes has captured interest in recent years, owing to their participation in a variety of redox processes. Besides, the study of compounds containing mixed N and S donor atoms has raised research interest in recent years due to their significant antifungal, antibacterial and anticancer activities. Finally, thioether ligands are of importance for coordination

chemists attempting to develop effective model complexes to mimic the active sites of sulfur-containing metalloproteins [16].

Among metal-based complexes, the platinum-based anticancer drugs such as cisplatin are well known and still widely used in the treatment of malignancies. However, Pt(II) drugs present severe side effects, toxicity, and different resistance mechanisms that have led to efforts to find better therapeutic alternatives [17–19]. As such, nickel (II), exhibiting the same d^8 electronic configuration, is a close analogue of platinum (II) but much more readily available. An advantage of Ni(II) is its ability to adopt a great variety of coordination geometries such as cis- or trans- square planar, tetrahedral, square-pyramidal, and octahedral, while Pt(II) only forms cis- or trans square planar complexes [20,21]. Furthermore, the biological properties of many nickel complexes are currently being investigated [22].

Herein, we present the synthesis nickel complexes with bis(benzimidazole)thio- and selenoether-based ligands (Figure 1), along with their characterization and *in vitro* anticancer activity. The modular architecture of this ligand family allows us to study different structural parameters such as the electronic and steric properties of the thioether functionality, the substituents in the alkyl chain connecting from the central nitrogen to the thioether moiety, and the replacement of the thioether functionality by a selenoether one.

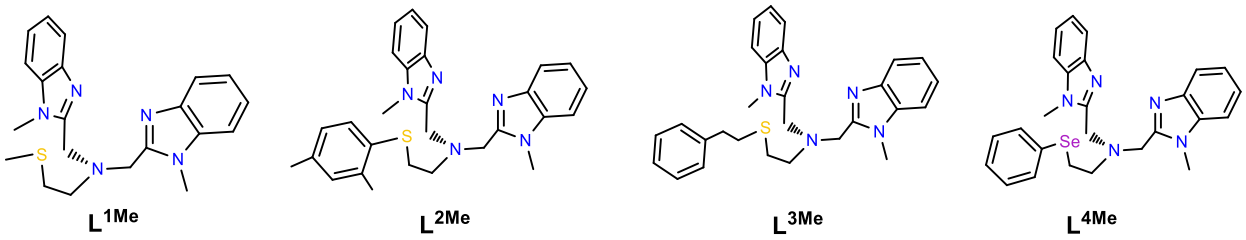

Figure 1. Structure of ligands.

2. Experimental

2.1. Reagents and techniques

Solvents and reagents were obtained from commercial suppliers and were used without further purification. $NiCl_2 \cdot 6H_2O$ was used as received from Aldrich. Mass spectra were obtained on a JEOL JMS-SX-102A mass spectrometer at an accelerating voltage of 10 kV, with a nitrobenzyl alcohol matrix and Xenon atoms at 6 keV (FAB^+) or a JEOL The AccuTOF JMS-T100LC (DART). NMR spectra were recorded on a JEOL Eclipse 300 spectrometer in $CDCl_3$ with tetramethylsilane as an internal standard. Melting points were determined on an Electrothermal Mel-Temp apparatus and are uncorrected. UV–Vis spectra were recorded on a Shimadzu UV-160U spectrophotometer. Elemental analyses were performed at the microanalytical facility of the Instituto de Química. Solid state magnetic susceptibility measurements were performed at room temperature using a MSB Evans balance; the appropriate diamagnetic corrections were applied using Pascal's constants [23]. Cyclic voltammetry measurements were made under N_2 or Ar in anhydrous CH_3CN, with a CH Instruments potentiostat–galvanostat equipped with a glassy carbon working electrode and a

platinum wire auxiliary electrode. Potentials were recorded versus a pseudoreference electrode of AgBr(s)/Ag(wire) immersed in 0.1 M NBu_4Br acetonitrile. In agreement with IUPAC convention, the voltammogram of the ferrocenium/ferrocene (Fc^+/Fc) system [24] was obtained to establish the values of half wave potentials ($E_{1/2}$) from the expression $E_{1/2} = (E_a + E_c)/2$.

2.2. Ligands synthesis

The synthesis of ligands **L1^{Me}** and **L2^{Me}** has been previously reported [15,18,25], along with their physical characterization. In addition, we prepared **L3^{Me}** and **L4^{Me}** in an analogous fashion to its aryl- and methylthioether analogs; it consists of the reaction of (2-phenylethylthio)ethylamine for **L3^{Me}** or (2-phenylseleno)ethylamine for **L4^{Me}** with two equivs. of 1-methyl-2-(chloromethyl)benzimidazole in the presence of base.

L3^{Me}. 1-Methyl-2-cloromethylbenzimidazole (1.20 g, 6.60 mmol), (2-phenylethylthio)ethylamine (0.61 g, 3.30 mmol), potassium carbonate (1.80 g, 13.33 mmol), and sodium iodide (50 mg, 0.33 mmol) were placed in 15 mL CH_3CN in a round bottom flask, and the mixture was heated to reflux for 5 h. The solution was then filtered through Celite, concentrated to dryness, and extracted with 3 x 10 mL of dichloromethane. The solution was concentrated to ca. 5 mL, and the concentrated solution was evaporated slowly to afford pale yellow crystals of **L3^{Me}** (0.71 g; 45%). Mp: 132-135 °C. IR (ATR): ν = 3057, 3026, 2944, 2920, 2808, 1672, 1613, 1511, 1475, 1454, 1438, 1399, 1330, 1285, 1206, 1173, 1121, 1097, 1029, 989, 938, 858, 798, 766, 740, 696, 540, 498, 435 cm^{-1}. DART-MS: *m/z* 470 $[M+1]^+$. ^1H NMR ($CDCl_3$, 300 MHz): δ = 7.70 (m, 2H, BzIm), 7.22 (m, 9H, Ph and BzIm), 6.99 (m, 2H, BzIm), 3.99 (s, 4H, BzIm-CH_2),

3.64 (s, 6H, BzIm-CH_3), 2.93 (t, 2H, N-CH_2), 2.62 (m, 4H, S-CH_2CH_2-Ph), 2.49 (m, 2H, S-CH_2) ppm. $^{13}C\{^1H\}$ NMR ($CDCl_3$, 75 MHz): δ 151.13 (BzIm), 142.20 (BzIm), 140.41 (BzIm), 136.21 (Ph), 128.54 (Ph), 128.49 (Ph), 126.37 (Ph), 122.98 (BzIm), 122.28 (BzIm), 119.83 (BzIm), 109.29 (BzIm), 54.16 (S-CH_2), 51.49 (N-CH_2), 36.23 (N-CH_2-Bzim), 33.45 (CH_2), 30.01 (N-CH_3), 29.87 (CH_2) ppm.

L4^{Me}. In a 100 mL round bottom flask, 1.20 g (6.60 mmol) 1-methyl-2-chloromethylbenzimidazole, 1.80 g (13.33 mmol) K_2CO_3, and 50 mg (0.33 mmol) of NaI were dissolved in CH_3CN, and the mixture was stirred at room temperature for 30 min; then 790 mg (3.33 mmol) of (2-phenylseleno)ethylamine were added, and the mixture was heated to reflux for 5 h. After cooling to room temperature, the solution was filtered through Celite and concentrated under reduced pressure. A colorless crystalline material started to deposit, the volume was reduced to ca. 3 mL under reduced pressure, and slow evaporation afforded **L4^{Me}** (1.14 g; 70%). Mp: 112–115 °C. IR (KBr): ν = 3057, 3028, 2922, 2807, 1611, 1511, 1475, 1454, 1437, 1398, 1358, 1330, 1289, 1234, 1206, 1173, 1147, 1121, 1097, 1029, 988, 939, 906, 860, 798, 762, 741, 696, 653, 569, 538, 499, 471, 440, 410 cm^{-1}.DART-MS: *m/z* 490 $[M+1]^+$. ^1H NMR ($CDCl_3$, 300 MHz): δ = 7.71 (m, 2H, BzIm), 7.26 (m, 6H, BzIm), 7.16 (d, 2H, Ph), 7.04 (m, 1H, Ph), 6.97 (m, 2H, Ph), 4.00 (s, 4H, BzIm-CH_2), 3.65 (s, 6H, BzIm-CH_3), 3.02 (t, 4H, N-CH_2CH_2-Se) ppm. $^{13}C\{^1H\}$ NMR ($CDCl_3$, 75 MHz): δ 151.03 (BzIm), 142.07 (BzIm), 140.29 (BzIm), 136.09 (Ph), 128.43 (Ph), 128.38 (Ph), 126.26 (Ph), 122.87 (BzIm), 122.17 (BzIm), 119.72 (BzIm), 119.72 (BzIm), 54.02 (S-CH_2), 51.39 (N-CH_2), 36.11 (NCH_2BzIm), 33.34 (NCH_3), 29.91 (CH_2), 29.75 (CH_2) ppm. ^{77}Se NMR ($CDCl_3$, 57 MHz): δ = 239 ppm.

2.3. Synthesis of complexes

Complexes **1**-**4** were prepared in a similar way. In the general procedure, acetonitrile solutions (10 mL) containing the corresponding ligand, **L1^{Me}** (0.53 mmol, 200 mg) for **1**, **L2^{Me}** (0.12 mmol, 60 mg) for **2**, **L3^{Me}** (0.43 mmol, 200 mg) for **3**, and **L4^{Me}** (0.61 mmol, 300 mg) for **4**, was added to methanolic solutions (5 mL) of $NiCl_2 \cdot 6H_2O$ in stoichiometric quantities. The mixtures were stirred for 3 h at room temperature, and volatile materials were then evaporated under reduced pressure, the solid obtained washed with 5 mL of diethylether, filtered, and dried under reduced pressure.

[Ni(L1^{Me})(H$_2$O)(Cl)]Cl (1). Green crystals of **1** in 68% yield suitable for X-ray structure determination were collected after slow evaporation in acetonitrile solution. *Anal.* Calcd. for $C_{23}H_{29}Cl_6N_5NiOS$ [Ni(**L1^{Me}**)(H_2O)(Cl)]Cl·$C_2H_2Cl_4$: N, 10.08; C, 39.75; H, 4.21; S, 4.61. Found: N, 10.28; C, 39.92; H, 4.31; S, 4.74. IR (ATR): 3395, 3273, 3175, 2929, 1656, 1613, 1482, 1455, 1328, 1298, 1248, 1218, 1087, 1008, 995, 926, 896, 766, 749, 644, 540, 437, 427 cm^{-1}. FAB^+ MS: *m/z* 472 [Ni(**L1^{Me}**)(Cl)]$^+$. UV-vis (MeCN): λ, nm (ε, M^{-1} cm^{-1}) 394 (59), 615 (62).

Ni$_2$(L2^{Me})$_2$(μ-Cl)$_3$]Cl (2). Green microcrystals of **2** in 40% yield suitable for X-ray structure determination were collected by filtration after then days of slow evaporation in acetonitrile solution. *Anal.* Calcd. for $C_{56}H_{68}Cl_4N_{10}Ni_2O_3S_2$ [Ni_2(**L2^{Me}**)$_2$(μ-Cl)$_3$]Cl·3H_2O: N, 11.18; C, 53.70; H, 5.47; S, 5.12. Found: N, 11.19; C, 53.59; H, 5.33; S, 4.88.). IR (ATR): 3304, 3202, 2948, 2934, 1616, 1504, 1480, 1451, 1329, 1296, 1250,

1103, 1016, 1008, 979, 932, 899, 875, 763, 745, 556, 427 cm^{-1}. FAB^+ MS: *m/z* 562 $[Ni(\mathbf{L2^{Me}})(Cl)]^+$. UV-vis (MeCN): λ, nm (ε, M^{-1} cm^{-1}) 303 (2671), 359 (321), 635 (14).

$[Ni_2(\mathbf{L3^{Me}})_2(\mu\text{-}Cl)_2][NICl_4]$ (3). Green microcrystals of **3** in 53% yield were collected by filtration after then days of slow evaporation in acetonitrile solution. *Anal.* Calcd. for $C_{56}H_{70}Cl_6N_{10}Ni_3O_4S_2$ $[Ni_2(\mathbf{L3^{Me}})_2(\mu\text{-}Cl)_2][NICl_4]$ ·$4H_2O$: N, 10.00; C, 48.04; H, 5.04; S, 4.58. Found: N, 10.24; C, 48.01; H, 5.08; S, 4.28. IR (ATR): 3060, 3025, 2944, 2930, 1613, 1498, 1482, 1453, 1326, 1295, 1151, 1127, 1103, 1007, 973, 926, 894, 782, 743, 697, 540, 431 cm^{-1}. FAB^+ MS: *m/z* 562 $[Ni(\mathbf{L3^{Me}})(Cl)]^+$. UV-vis (MeCN): λ, nm (ε, M^{-1} cm^{-1}) 395 (46), 636 (41).

$[Ni_2(\mathbf{L4^{Me}})_2(\mu\text{-}Cl)_2][NICl_4]$ (4). Green crystals of **4** in 54% yield suitable for X-ray structure determination were collected by slow evaporation in tetrachloroethane-methanol solution. *Anal.* Calcd. for $C_{56}H_{58}Cl_{14}N_{10}Ni_3Se_2$ $[Ni_2(\mathbf{L4^{Me}})_2(\mu\text{-}Cl)_2][NICl_4]$ ·$2C_2H_2Cl_4$: N, 8.23; C, 39.53; H, 3.44. Found: N, 8.12; C 39.63; H, 3.54. IR (ATR): 3356, 3053, 2942, 2912, 1616, 1500, 1481, 1453, 1327, 1294, 1101, 1108, 893, 783, 740, 684, 538, 430 cm^{-1}. FAB^+ MS: *m/z* 582 $[Ni(\mathbf{L4^{Me}})(Cl)]^+$. UV-vis (MeCN): λ, nm (ε, M^{-1} cm^{-1}) 304 (4656), 414 (70), 651 (28).

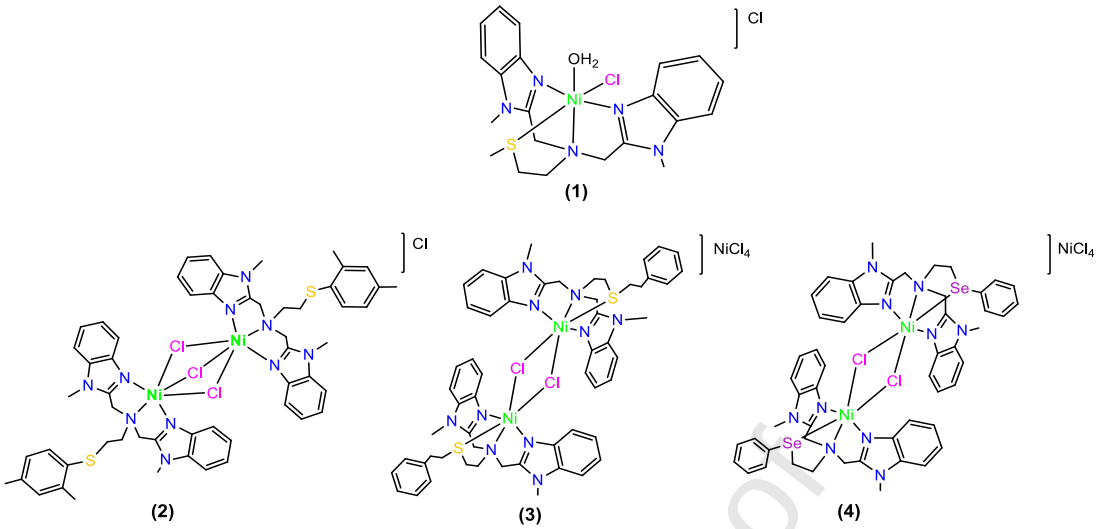

Figure 2. Nickel complexes **1**-**4**.

2.4. X-ray structure determination

X-ray diffraction data for **1** and **2** were collected on a Bruker SMART or a SMART APEX DUO CCD diffractometer with Mo Kα radiation (λ = 0.71073 Å) at 298(2) K for **1** and 100(2) K for **2**. Frames were collected by omega scans, integrated using the SAINT software, and corrected for semiempirical absorption (SADABS) [26]. The structures were solved by direct methods (SHELXT) [27], and refined by full-matrix least-squares on F^2 with SHELXL-97 [28] using the SHELXLE GUI [29]. Weighted R-factors, Rw, and all goodness-of-fit indicators, S, were based on F^2. The observed criterion of $F^2 > 2\sigma F^2$ was used only for calculating the R-factors. In **2** the disordered imidazole moiety, disordered chlorine anion and two disordered water molecules were refined using geometry (SADI, DFIX, SAME) and Uij restraints (SIMU, RIGU, ISOR, EADP) using free variable for occupancy implemented in SHELXL [28]. The occupancy ratio for majority

position and second position in imidazole, chlorine atom and water molecules are 55/45, 91/9 and 63/37 respectively.

Crystals of **3** and **4** were mounted on a glass fiber and crystallographic data were collected with an Oxford Diffraction Gemini "A" diffractometer with a CCD area detector ($\lambda_{MoK\alpha}$ = 0.71073 Å) at 130 K. The double pass method of scanning was used to exclude any noise [30]. The collected frames were integrated by using an orientation matrix determined from the narrow frame scans. Final cell constants were determined by a global refinement; collected data were corrected for absorbance by using analytical numeric absorption correction using a multifaceted crystal model based on expressions upon the Laue symmetry with equivalent reflections [31]. Structures solutions and refinement were carried out with the SHELXS-2014 [27] and SHELXL-2014 [28] packages. WinGX v2018.3 [32] software was used to prepare material for publication. Full-matrix least-squares refinement was carried out by minimizing $(Fo^2 - Fc^2)^2$.

For all complexes, all non-hydrogen atoms were refined anisotropically. H atoms attached to C atoms were placed in geometrically idealized positions and refined as riding on their parent atoms, with C–H = 0.95 – 1.00 Å and with U_{iso}(H) = 1.2U_{eq}(C) for aromatic, methylene and methine groups, and 1.5U_{eq}(C) for methyl groups. Crystallographic data for all complexes are presented in Table 1. The crystallographic data for the structures reported in this paper has been deposited with the Cambridge Crystallographic Data Centre as supplementary publication no. CCDC 2008985, 2008986, 2009133, and 2009134. Copies of the data can be obtained free of charge on

application to CCDC, 12 Union Road, Cambridge, CB2 1EZ, UK (fax: (+44) 1223-336-033, e-mail: deposit@ccdc.cam.ac.uk).

Table 1. Summary of crystallographic data for **1**-**4**.

	1	**2**	**3**	**4**
Empirical formula	$C_{21}H_{29}Cl_2N_5NiO_3S$	$C_{56}H_{68}Cl_4N_{10}Ni_2O_3S_2$	$C_{62}H_{71}Cl_6N_{13}Ni_3S_2$	$C_{62}H_{64}Cl_{26}N_{10}Ni_3Se_2$
Formula weight	561.16	1252.54	1451.26	2204.98
Temperature	298(2) K	100(2) K	130(2) K	130(2) K
Wavelength	0.71073 Å	0.71073 Å	0.71073 Å	0.71073 Å
Crystal system	Triclinic	Monoclinic	Monoclinic	Triclinic
Space group	P-1	C2/c	P 21/c	P -1
Unit cell dimensions	a= 9.772(2) Å b= 11.675(3) Å c= 12.607(3) Å α = 80.808(6)° β = 71.554(6)° γ = 71.654(6)°	a=22.1478(13) Å b=16.0954(9) Å c=15.7892(9) Å α = 90° β = 94.5402(12)° γ = 90°	a=19.1172(16) Å b = 21.037(3) Å c=16.3655(9)Å α = 90° β = 95.512(6)° γ = 90°	a=13.2046(15) Å b=15.5353(16) Å c=23.247(2) Å α = 76.998(9)° β = 79.473(9)° γ = 68.262(10)°
Density (calculated)	1.442 mg/m^3	1.483 mg/m^3	1.471 mg/m^3	1.707 mg/m^3
Volume	1292.2(5) Å^3	5610.8(6) Å^3	6551.3(11) Å^3	4290.0(8) Å^3
Z	2	4	4	2
Absorption coefficient	1.070 mm^{-1}	0.991 mm^{-1}	1.212 mm^{-1}	2.355 mm^{-1}
F(000)	584	2616	3008	2200
Crystal size	0.38x0.136x0.098 mm^3	0.400x0.139x0.062 mm^3	0.270x0.130x0.070 mm^3	0.270x0.170x0.120 mm^3
Reflections collected	19510	27398	39705	47896
Independent reflections	4709 [R(int) = 0.0303]	6448 [R(int) = 0.0423]	15899 [R(int) = 0.0585]	20268 [R(int) = 0.1042]
Absorption correction	Multi-scan	None	Analytical	Analytical
Refinement method	Full-matrix least-squares on F^2	Full-matrix least-squares on F^2	Full-matrix least-squares on F^2	Full-matrix least-squares on F^2
Data / restraints / parameters	4709 / 13 / 334	6448 / 597 / 509	15899 / 0 / 782	20268 / 0 / 932
Goodness-of-fit on F^2	1.078	1.026	1.056	1.021
Final R indices [I>2sigma(I)]	R1 = 0.0402 wR^2 = 0.1119	R1 = 0.0321 wR^2 = 0.0749	R1 = 0.0868 wR^2 = 0.2160	R1 = 0.0721 wR^2 = 0.1632
R indices (all data)	R1 = 0.0444 wR^2 = 0.1164	R1 = 0.0450 wR^2 = 0.0818	R1 = 0.1105 wR^2 = 0.2415	R1=0.1539 wR^2 = 0.2137

2.5. Cytotoxicity assay

Two human cancer cell lines: HeLa (cervical carcinoma) and SKLU-1 (human lung adenocarcinoma) and a normal cell line HEK-293 (human embryonic kidney) were provided by the National Cancer Institute (USA). Cells were cultured in a RPMI-1640

medium (RPMI Medium 1640 (1×), Gibco, Gaithersburg, Maryland) supplemented with 10% fetal bovine serum (FBS, Invitrogen, Carlsbad CA), L-glutamine (2 µM), penicillin G (100 u/mL), and streptomycin sulfate (100 µg/mL) at 37°C with 5% v/v CO_2. Biological assays were carried out in a 96 well plates at 5000 cells/well. After 24 hours, the cells were treated with increasing concentrations of the complexes (1, 5, 10, 25, 50, 75 and 100 µM). Cell viability was evaluated after 72 h incubation with complexes.

After treatments, culture media was replaced by 100 µL of MTT (3-(4,5-dimethylthiazol-2-yl)-2,5-diphenyltetrazolium bromide) to a final concentration of 0.33 mg/mL dissolved in culture media and incubated at 37 °C with 5% CO_2 for 1 h in the dark. Supernatant was removed and replaced with DMSO to dissolve formazan crystals. Absorbance value was measured at 570 nm. Experiments were done in triplicate. IC_{50} was calculated from three independent experiments using GraphPad Prism 7.00 (GraphPad Software, La Jolla California USA). Percentage of cell viability was calculated in comparison with control cells.

3. Results and discussion

3.1. Ligand synthesis

The synthesis of bisbenzimidazole-chalcogenoether mixed ligands (Scheme 1) was accomplished following a route similar to published methods [18,25,33]. The corresponding nickel complexes **1–4** were prepared by adding one equivalent of ligand in acetonitrile solution to solutions of $NiCl_2{\cdot}6H_2O$ in methanol. In all cases, the yellow

solutions of the ligands changed color to dark green immediately after addition of nickel(II) chloride.

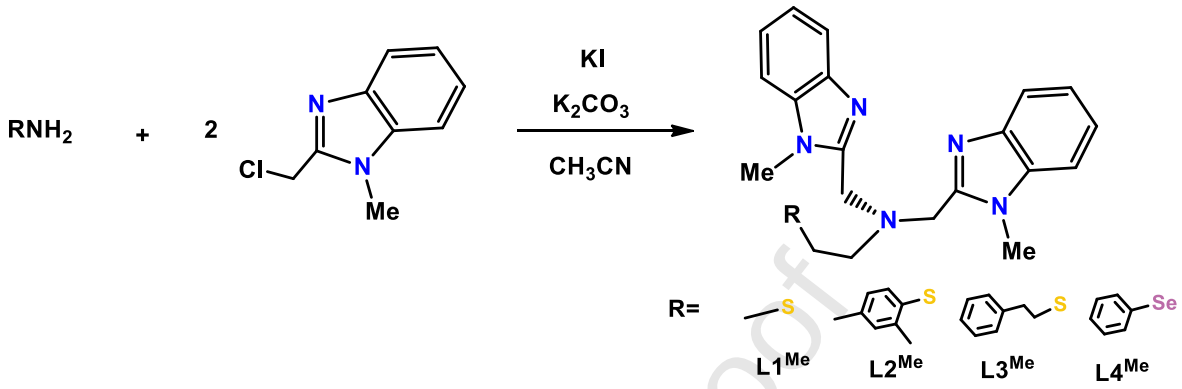

Scheme 1. General procedure for ligand synthesis

3.2. Characterization and solid-state structures of nickel complexes

The complexes were characterized by various analytical and spectroscopic techniques. Characterization of the isolated complexes in the solid state by combustion analysis matches the proposed formulations. IR spectra present the bis(2-methylbenzimidazolyl)amine ligand-derived C–H stretching bands between 3200 and 2900 cm^{-1}, as well as aromatic C–C and C–N stretches around 1450–1275 cm^{-1}. All the nickel(II) complexes **1**-**4** were found to be electron paramagnetic resonance (EPR) silent.

Solid state magnetic susceptibility measurements were performed on **1**-**4** at room temperature; values for the effective magnetic moment and magnetic susceptibility are given in Table 2. In all cases, the positive value of χ_A indicates that the nickel complexes are paramagnetic [23]. The μ_{eff} value of 3.04 Bohr Magnetons (BM) for **1** is close to the spin-only value (μ_{eff} =2.83 BM) at room temperature for a magnetically isolated Ni(II)

system, and is typical for paramagnetic octahedral Ni(II) complexes with d^8 configuration. The value agrees with results reported previously on similar Ni(II) complexes [34–36]. Likewise, the values of 4.19, 4.52 and 4.75 for the other compounds, are slightly lower than the expected value for a system with 4 unpaired electrons (4.90 BM), which in related dinuclear Ni(II) complexes indicates a weak antiferromagnetic coupling between the two paramagnetic metal ions [37].

Table 2. Magnetic parameters of complexes **1–4**

Compound	Magnetic parameters	
	μ_{eff} (BM)	χ_A (emu mol^{-1})
1	3.04	3.91×10^{-3}
2	4.19	7.42×10^{-3}
3	4.52	8.65×10^{-3}
4	4.75	9.56×10^{-3}

The coordination environment around the nickel centers in the complexes was established by single-crystal X-ray diffraction. Crystals of **1**, **2** and **3** (acetonitrile), as well as, **4** (tetrachloroethane/methanol), suitable for diffraction studies were obtained by slow evaporation of saturated solutions. In all cases the Ni(II) ions display slightly distorted octahedral geometries; with the exception of **1**, complexes **2**, **3** and **4** are dimers with chloride bridges between the two metal centers. Depiction of the solid-state structures with atom numbering schemes are presented in Figure 3 for **1**, Figure 4

for **2**, Figure 5 for **3,** and Figure 6 for **4**. Selected bond distances (Å) and angles (°) are presented in Table 3.

Complex **1** crystallizes in the triclinic space group *P*-1, the Ni(II) ion coordinated by one thioether sulfur atom, two benzimidazole nitrogen atoms, the nitrogen atom of the tertiary amine, one chloride, and a molecule of water, with an outer-sphere chloride ion. In contrast, complexes **2**, **3** and **4** reveal dimeric species. In the case of **2**, the asymmetric unit is comprised of [Ni(**L2**$^{\mathbf{Me}}$)$(Cl)_2$] (Figure 4 A) and the nickel center is coordinated by the three ligand-derived nitrogen atoms; notably, the thioether sulfur atom does not coordinate to the Ni(II) ion. As is the case with **1**, the counterion is an outer-sphere chloride. In **3** and **4**, the chloride-bridged cationic dimers are accompanied by tetrachloronickelate dianions; in the cations, the Ni(II) centers are coordinated by all N and S/Se donors. Complex **2** has three bridging chlorides and a Ni···Ni distance of 3.0818(5) Å, while in **3** and **4** the Ni(II) centers share two bridging chlorides at Ni···Ni distances of 3.447(7) and 3.480(6) Å respectively.

In **2**, the three coordinated N atoms are in trans positions relative to the chloride bridges, with the Ni-N_{amine} distances 0.163 and 0.193 Å longer than each of the Ni-N_{Bnz} bonds. For **3** and **4** that only have two chloride bridges, the Ni-N_{amine} bonds are also longer than the corresponding Ni-N_{Bnz} bond lengths; among these (Ni-N_{Bnz}), the ones that are trans relative to the bridging chlorides are the longest, likely reflecting a trans influence. In general, the bond lengths agree well with those reported for octahedral nickel (II) complexes [38].

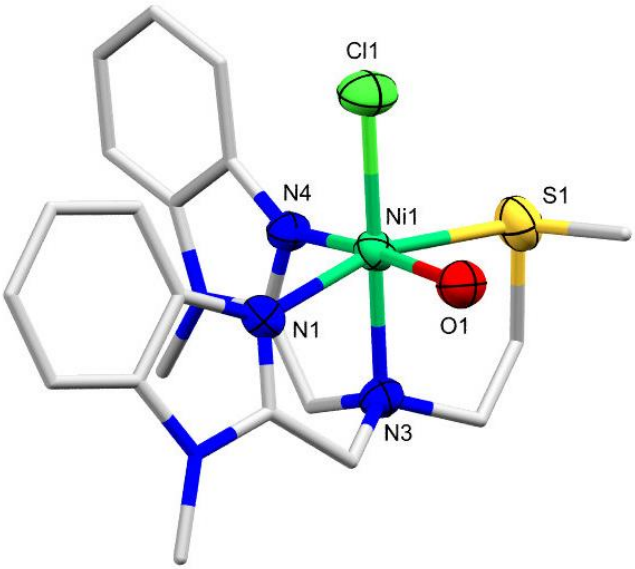

Figure 3. Mercury diagram of **1** at the 50% probability level, hydrogen atoms and anion are omitted, C and N atoms not coordinated to Ni shown as wireframe for clarity. Color code: C, gray; S, yellow; O, red; N, blue; Cl, lime; Ni, green.

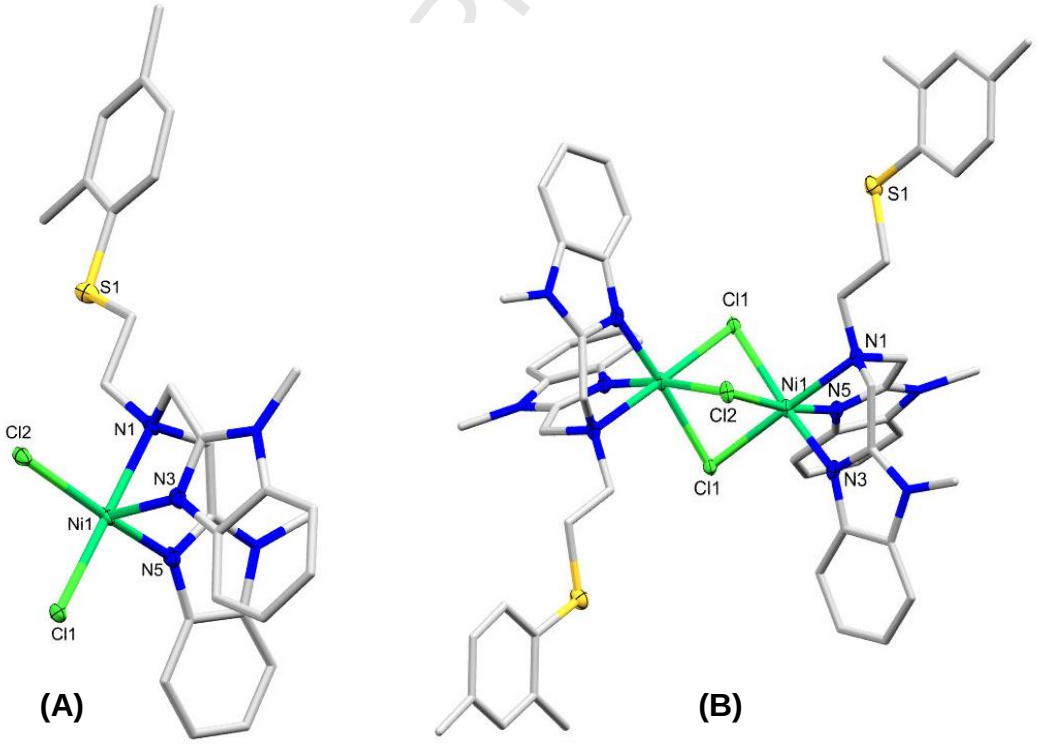

Figure 4. Mercury diagram of asymmetric (A) and dimeric (B) unit of **2** at the 50% probability level; hydrogen atoms and anion are omitted for clarity.

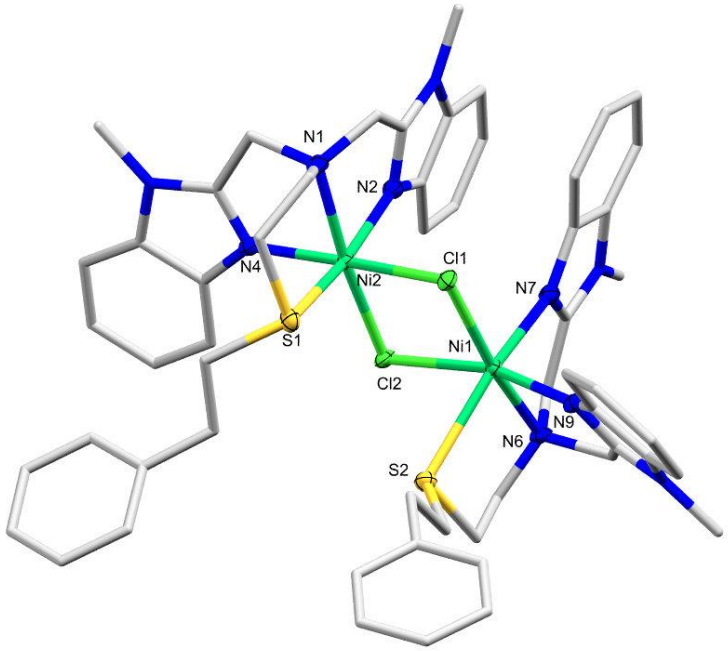

Figure 5. Mercury diagram of **3** at the 50% probability level, hydrogen atoms and anion are omitted for clarity.

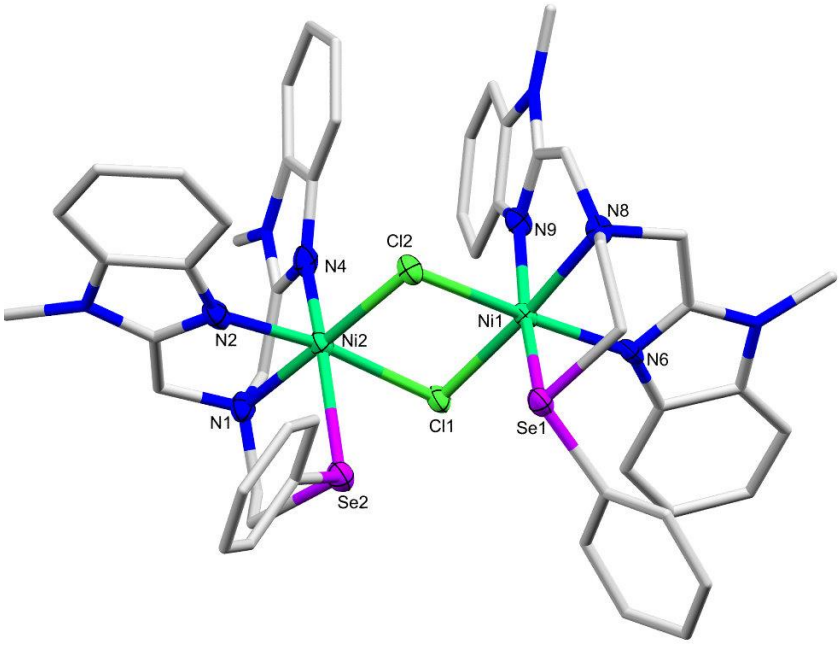

Figure 6. Mercury diagram of **4** at the 50% probability level, hydrogen atoms and anion are omitted for clarity. Color code: Se, purple.

Table 3. Selected bond distances (Å) and angles (°) for **1**-**4**.

1		**2**	
Ni1-Cl1	2.358(1)	Ni1-N1(Amine)	2.212(2)
Ni-N1(BzIm)	2.062(3)	Ni-N3(BzIm)	2.049(8)
Ni-N4(BzIm)	2.048(2)	Ni1-N5(BzIm)	2.019(2)
Ni-N3(Amine)	2.201(2)	Ni1-Cl1	2.399(6)
Ni1-S1	2.490(1)	Ni1-Cl2	2.460(6)
N1-O1	2.121(2)		
		Cl1-Ni1-Cl2	84.75(15)
N1-Ni1-N3	78.26(8)	Cl1(#1)-Ni1-Cl2	83.50(15)
N1-Ni1-N4	90.36(8)	Cl1-Ni1-Cl1(#1)	85.58(19)
N3-Ni1-N4	81.32(8)	Ni1-Cl1-Ni1(#1)	78.70(17)
Cl1-N1-S1	95.91(3)	Ni1(#1)-Cl2-Ni1	76.50(2)
Cl1-Ni1-O1	86.53(6)	N5-Ni1-N3	91.9(3)
Cl1-Ni1-N4	98.19(6)	N1-Ni1-N5	81.51(6)
S1-Ni1-N3	83.95(6)	N1-Ni1-N3	77.7(3)
S1-Ni1-N4	89.30(6)	Cl1-Ni1-N5	100.40(5)
S1-Ni1-O1	92.06(6)	Cl1-Ni1-N3	100.2(3)
		N5-Ni1-Cl1(#1)	91.38(5)
		N1-Ni1-Cl1(#1)	96.45(4)
		Cl2-Ni1-N3	92.60(3)
		Cl2-Ni1-N1	93.55(4)

3		**4**	
Ni1-N9(BzIm)	2.016(4)	Ni1-N6(BzIm)	2.042(5)
Ni1-N7(BzIm)	2.059(4)	Ni1-N9(BzIm)	2.039(6)
Ni1-N6(Amine)	2.160(4)	Ni1-N8(Amine)	2.162(6)
Ni1-S2	2.560(13)	Ni1-Se1	2.589(1)
Ni1-Cl1	2.372(12)	Ni1-Cl1	2.359(2)
Ni1-Cl2	2.439(12)	Ni1-Cl2	2.487(2)
Ni2-N4(BzIm)	2.019(4)	Ni2-N4(BzIm)	2.016(6)
Ni2-N2(BzIm)	2.050(4)	Ni2-N2(BzIm)	2.055(5)
Ni2-N1(Amine)	2.146(4)	Ni2-N1(Amine)	2.170(5)
Ni2-S1	2.475(13)	Ni2-Se2	2.555(1)
Ni2-Cl1	2.479(12)	Ni2-Cl1	2.504(2)
Ni2-Cl2	2.360(11)	Ni2-Cl2	2.373(2)
N9-Ni1-N7	96.89(15)	Se1-Ni1-Cl1	98.21(5)
N9-Ni1-N6	83.16(15)	Se1-Ni1-Cl2	79.16(5)
N7-Ni1-N6	79.12(15)	Se1-Ni1-N6	93.1(2)
N9-Ni1-Cl1	99.10(11)	Se1-Ni1-N8	86.4(1)
N7-Ni1-Cl1	92.25(11)	Cl1-Ni1-Cl2	88.76(6)
N7-Ni1-Cl2	95.57(11)	Cl1-Ni1-N6	99.7(2)
N6-Ni1-Cl2	90.96(11)	Cl1-Ni1-N9	96.3(2)
Cl1-Ni1-Cl2	88.79(4)	Cl2-Ni1-N8	89.5(1)
N9-Ni1-S2	88.37(11)	Cl2-Ni1-N9	93.2(2)
N6-Ni1-S2	83.61(11)	N6-Ni1-N8	82.6(2)

Cl1-Ni1-S2	104.79(4)	N6-Ni1-N9	92.4(2)
N4-Ni2-N2	92.34(15)	N8-Ni1-N9	78.8(2)
N4-Ni2-N1	82.87(15)	Se2-Ni2-Cl1	78.51(4)
N2-Ni2-N1	79.88(15)	Se2-Ni2-Cl2	96.81(5)
N4-Ni2-Cl2	98.94(11)	Se2-Ni2-N1	86.6(1)
N2-Ni2-Cl2	93.02(11)	Se2-Ni2-N2	96.7(2)
N4-Ni2-S1	92.03(11)	Cl1-Ni2-Cl2	88.04(6)
N1-Ni2-S1	84.88(11)	Cl1-Ni2-N1	90.2(1)
Cl2-Ni2-S1	102.01(4)	Cl1-Ni2-N4	91.4(2)
N2-Ni2-Cl1	96.60(11)	Cl2-Ni2-N2	99.6(2)
N1-Ni2-Cl1	91.29(11)	Cl2-Ni2-N4	96.3(2)
Cl2-Ni2-Cl1	88.11(4)	N1-Ni2-N2	82.4(2)
S1-Ni2-Cl1	77.32(4)	N1-Ni2-N4	79.9(2)
		N2-Ni2-N4	91.5(2)

Symmetry transformations used to generate equivalent atoms for **2** (#1): -x+1,y,-z+1/2

3.3. Solution characterization of nickel complexes

The nickel complexes **1**-**4** are soluble in polar solvents but only sparingly soluble in non-polar solvents such as dichloromethane. ^{1}H NMR spectra could not be obtained in view of the paramagnetic character of the complexes. In the positive-ion fast atom bombardment mass spectrometry (FAB^{+}-MS), for all cases a signal corresponding to [Ni(**L**)(Cl)]$^{+}$ was detected (Figure S9 in the Supporting Information), *m/z* 472 for **1**, 562 for **2** and **3**, and 582 for **4**, that for complexes **3** and **4** corresponding to half the molecular weight of the putative dimer expected. The results of FAB^{+}-MS, and osmometry determinations by vapor diffusion of acetonitrile solutions, leads us to propose a monomeric nature in solution for all complexes in the form of [Ni(**L**)(Cl)]$^{+}$. The ligands may coordinate through all donor atoms to the Ni(II) centers, but the chloride bridges are broken.

Optical spectra for the complexes in acetonitrile or methanol are shown in Figure 7, with relevant electronic absorption parameters summarized in Table 4. All complexes have similar spectra in MeCN and MeOH, the principal differences are the intensity of the signals, with smaller molar absorptivities in methanol. In all cases the strong absorption bands below 300 nm were assigned as intraligand transitions. The electronic spectral diagram shows bands at ~300 and 400 nm for **2** and 4, assigned as Ligand-to Metal Charge Transfer (LMCT) from the coordinated chalcogens (E = S or Se) to the Ni(II) ions, $E_{p\sigma} \rightarrow$ Ni and $E_{p\pi} \rightarrow$ Ni, respectively. For **1** and **3**, only the one assigned to $E_{p\pi} \rightarrow$ Ni is observed at ~395 nm. The bands observed for **2** and **4** are intense, reflecting a high degree of electronic delocalization between the metal orbitals and the thio- or selenoether donors, which can be directly related to a high degree of covalency of the M−E bonds [39]. The broad signals observed from 500 nm to 800 nm were assigned to weak *d–d* bands (ε < 100), which are typical for octahedral Ni(II) complexes [40]. As a consequence of an increasing electron donating ability in the ligand by the different substitution in the amine, the *d–d* band for complex **1** at 615 nm is red shifted to 635, 636 and 651 nm in **2**, **3**, and **4** respectively [41]. The optical parameters summarized in Table 4 are consistent with previously reported Ni complexes in octahedral geometry [38,42]. It is important to emphasize that in the solid state **2** does not present M-S ligation, but since in the UV-vis spectrum the characteristic bands of M-S transitions are present, it appears that in solution the chalcogen atom is coordinated, in agreement with the mass spectrometry and osmometry measurements.

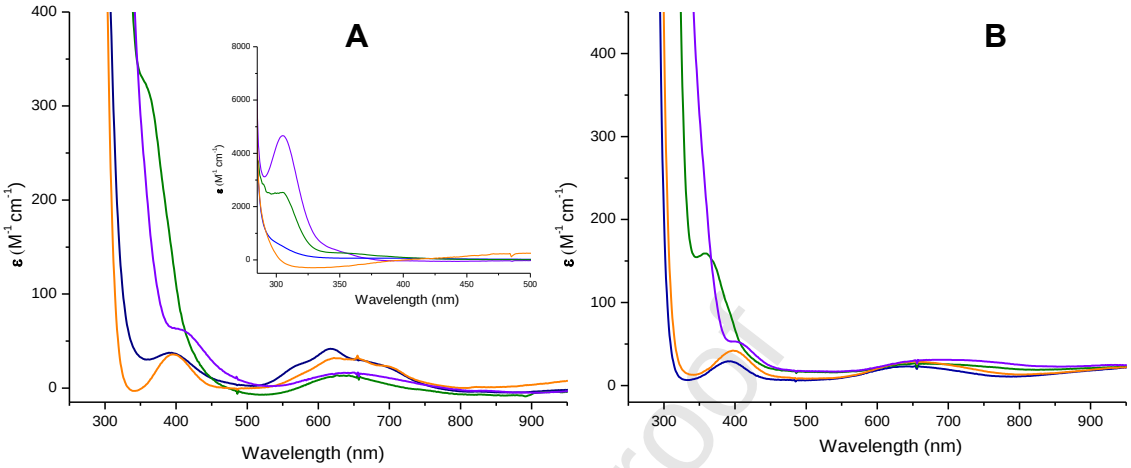

Figure 7. UV–Visible spectra of complexes **1** (blue line), **2** (green line), **3** (orange line) and **4** (purple line) in MeCN (Panel A) and MeOH (Panel B).

Table 4. Optical parameters of complexes **1–4**

Compound	Optical parameters λ (nm), [ε (M^{-1} cm^{-1})]		
	Acetonitrile	Methanol	Assignment
1	394 [42] 615 [45]	392[30] 647 [23]	Spπ → Ni *d–d*
2	303 [2550] 359 [317] 635 [14]	359 [200] 670 [26]	Spσ → Ni Spπ → Ni *d–d*
3	395 [36] 636 [32]	397 [42] 652 [29]	Spπ → Ni *d–d*
4	304 [4679] 414 [62] 651 [19]	404 [53] 693 [31]	Sepσ → Ni Sepπ → Ni *d–d*

3.4. Electrochemical Studies

Characterization of the ligands by cyclic voltammetry at a concentration of 1 mm in acetonitrile solution, and a scan rate of 0.100 V s^{-1} revealed that for all **L1^{Me}–L4^{Me}**, no processes are observed between -2.5 and 0.0 V. In the range of 0.3 to 1.2 V several oxidation processes are presented, which are distinct from those of the metal-centered redox process (Figure S14 in the Supporting Information). Cyclic voltammograms of the Ni(II) complexes are shown in Figure 8. The redox potentials were calibrated relative to that of the ferrocene/ferrocenium (Fc/Fc^{+}) redox couple in MeCN, and the corresponding potential peaks for the complexes are presented in Table 5.

When the potential scan was started from open circuit potential in the cathodic direction, one reduction process labeled I_c was recorded for all complexes between -1.4 and -1.7 V, assigned to the Ni(II)/Ni(I) couple. Scans in the anodic direction reveal one oxidation process I_a for **2** and **4** (Figure 8 A), which is not present for **1** and **3** (Figure 8 B). The redox wave (I_c/I_a) for **2** exhibited a quasi-reversible ($E_{1/2}$ = -1.39 V) feature with a peak separation of 140 mV (larger than the value of 57 mV accepted for a reversible system). A second oxidation wave (II_a) is observed for **1**, **3**, and **4** that can be assigned to the a Ni(I)/Ni(II) oxidation process associated with large structural changes, or to the anodic desorption of Ni(0) deposited in the electrode surface [43].

It is important to emphasize that in most reports regarding related dimeric Ni(II) complexes, electrochemical reduction to the corresponding Ni(I) species was not observed, and only in a few instances has this been reported as an irreversible process

at more negative potentials [39]. This supports the notion that the complexes are monomeric in acetonitrile solution.

Table 5. Redox potentials (V vs Fc/Fc^{+}) for Ni(II) complexes [1 mM] in MeCN.

	Compound				Assignment
	1	**2**	**3**	**4**	
I_C	-1.680	-1.458	-1.603	-1.532	Ni(II) ⟶ Ni(I)
I_A	--	-1.315	--	-1.413	Ni(I) ⟶ Ni(II)
II_A	-0.267	--	-0.508	-0.443	Ni(I) ⟶ Ni(II) or Ni(0) ⟶ Ni(II)
III_A	0.799	0.837	0.813	0.684	Ligand oxidation

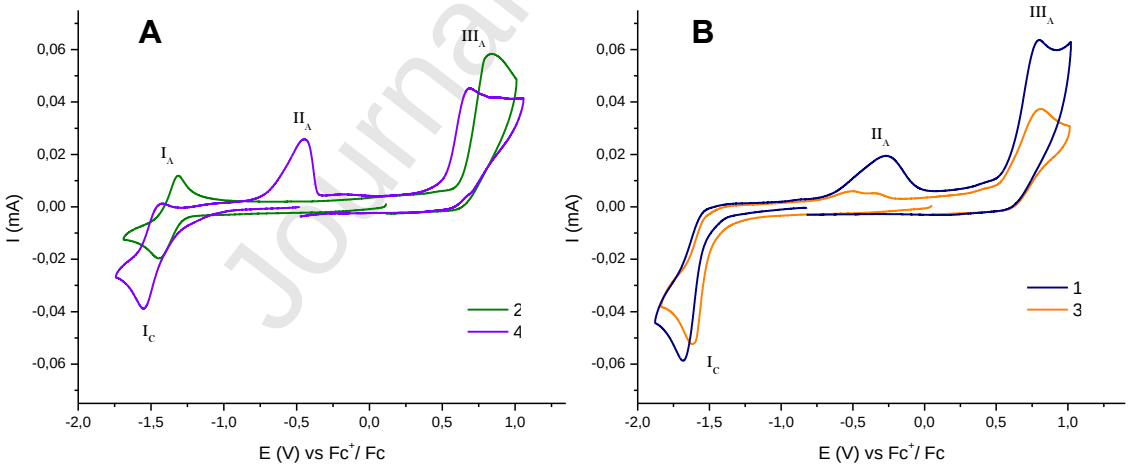

Figure 8. Cathodic CV of **1**-**4** (1 mM in 0.1 M NBu_4PF_6-MeCN, glassy carbon electrode) at a scan rate of 0.1 V s^{-1}.

3.5. Cytotoxicity studies

The stability of complexes in aqueous solution was monitored for 72 h (Figure S15, Supporting Information) by UV-vis spectroscopy, and the unchanged pattern of the spectra indicates that the compounds are stable for this period of time, which is the duration of the biological assays. The cytotoxicity of the ligands tends to be negligible towards cancer cell lines, based on previous reports [18,44].

The cytotoxicity of **1**-**4** complexes was screened against SK-LU-1 (human lung adenocarcinoma), HeLa (human cervical carcinoma) and HEK-293 (non-tumoral human embryonic kidney) cell lines using an MTT assay, which measures mitochondrial succinate dehydrogenase activity as an indicator of cell viability against human-derived cell lines. The cytotoxicity of these cell lines when exposed to increasing concentrations of the complexes for 72 hours was expressed as percentage cell viability relative to a control group, and then transformed to the corresponding 50% inhibitory concentration (IC_{50}) value. These data are summarized in Table 6, and were compared with cisplatin as reference. The nickel salt $NiCl_2$ and an analogous copper complex [Cu(**L3^{Me}**)(Cl)]Cl (**CuL3^{Me}**), synthesized from copper chloride and **L3^{Me}** are also presented to get a sense of the relative cytotoxicities for different metal ions with this class of ligands.

As shown in Table 6, **1** and **4**, as well as the nickel salt $NiCl_2$ are inactive against all tested cell lines with IC_{50} values > 100 µM. In contrast, **2** and **3**, and the cupric analogue **CuL3^{Me}** present moderate cytotoxicity in the tested cell lines. As for the two kinds of cancer cells, the cytotoxic effect of the copper complex is lower than that of cisplatin

but is still higher than that of the nickel complexes **2** and **3**. An analysis of the substituents on the amine group in the ligand for complexes **1**-**4** indicates that apparently the presence of an aromatic ring (in **2** and **3**), increases the cytotoxicity against the tested cell lines. The opposite effect was observed for the methyl group of **1**, or the change from S to Se in **4**.

Selectivity toward the SK-LU-1 and HeLa cell lines are observed compared to the non-tumoral HEK-293 cell line for all complexes, expressed as index values in Table 6. Specifically, complex **3** reduces more the viability of cancer cells compared with non-tumoral cells, exhibiting a nearly threefold selectivity, in contrast with its copper analogue. Considering the different cytotoxic activities and selectivities determined for the nickel and copper complexes, the identity of the metal is critical in the efficacy of anticancer metallodrugs as already reported [17].

Table 6. IC_{50} values [μM] for compounds on lung (SK-LU-1) and cervical (HeLa) cancer cell lines and non-tumoral (HEK-293) cell line at 72 h.

Compound	*IC_{50} (μM)*				
	HEK-293	**SK-LU-1**	**S.I.**	**HeLa**	**S.I.**
1	> 100	> 100	--	> 100	--
2	37 ± 0.1	25 ± 0.1	1.5	37 ± 0.1	1
3	48 ± 0.1	18 ± 0.2	2.7	19 ± 0.2	2.5
4	> 100	> 100	--	> 100	--
$NiCl_2$	> 100	> 100	--	> 100	--
$CuL3^{Me}$	10 ± 0.3	6 ± 0.1	1.6	11 ± 0.1	0.9
Cisplatin	10 ± 0.7 [45]	3.4 ± 0.5[a] [46]	2.9	4.9 ± 0.3 [47]	2.0

[a] IC_{50} at 48h. Values are given as the mean ±SD. Selectivity indexes (S.I.) calculated as ratio between IC_{50} values related to HEK-293 and cancer cell lines.

4. Conclusions

We have synthesized and characterized nickel complexes with bis(benzimidazole)thio- and selenoether-based ligands. In the solid state **2**, **3** and **4** are bimetallic complexes, but the spectroscopic characterization of the all complexes is consistent with a monometallic formulation in solution. The four complexes differ in the substituent of the thioether arm in **1**-**3**, and selenoether in the case of **4**. These modifications allowed us to investigate the role of the aromatic or methyl group as well as the role of the change from S to Se, in the electronic and redox properties, and in the biological activity of these complexes. **1** and **4**, as well as the nickel salt $NiCl_2$ are inactive against all tested cell lines. Based on the cytotoxic effect of the complexes, it is noteworthy that complexes **2** and **3** have an efficiency that, although lower than that of cisplatin against the human cancer cell lines (HeLa, SK-LU-1), is promising due to the relatively selectivity against healthy cells (HEK-293) in contrast with the copper analogue **CuL3^{Me}**.

Acknowledgements

The authors thank Javier Pérez, Luis Velasco, and María del Carmen García for mass spectrometry, María de la Paz Orta for combustion analysis, and Virginia Gómez-Vidales for EPR measurements, Conacyt (Beca 889015) and DGAPA-PAPIIT (IN217020) for financial support.

References

[1] N.N.M. Ishak, J. Jamsari, A.Z. Ismail, M.I.M. Tahir, E.R.T. Tiekink, A. Veerakumarasivam, T.B.S.A. Ravoof, Synthesis, characterisation and biological

studies of mixed-ligand nickel(II) complexes containing imidazole derivatives and thiosemicarbazide Schiff bases, J. Mol. Struct. 1198 (2019) 1268–1278. doi:10.1016/j.molstruc.2019.126888.

[2] S. Nashaat, M.A. Henen, S.M. El-messery, H. Eisa, Synthesis, state-of-the-art NMR-binding and molecular modeling study of new benzimidazole core derivatives as Pin1 inhibitors: Targeting breast cancer, Bioorg. Med. Chem. 28 (2020) 115495. doi:10.1016/j.bmc.2020.115495.

[3] M.T. Maghraby, O.M.F. Abou-ghadir, S.G. Abdel-moty, A.Y. Ali, O.I.A. Salem, Novel class of benzimidazole-thiazole hybrids: the privileged scaffolds of potent anti-inflammatory activity with dual inhibition of cyclooxygenase and 15-lipoxygenase enzymes, Bioorg. Med. Chem. 28 (2020) 115403. doi:10.1016/j.bmc.2020.115403.

[4] R. Wubulikasimu, Y. Yang, F. Xue, X. Luo, D. Shao, Y. Li, R. Gao, W. Ye, Synthesis and biological evaluation of novel benzimidazole derivatives bearing a heterocyclic ring at 4/5 position, Bull. Korean Chem. Soc. 34 (2013) 2297–2304. doi:10.5012/bkcs.2013.34.8.2297.

[5] M.A. Redayan, W.B. Ali, A.M. Mohammed, Synthesis, characterization and antibacterial evaluation of some novel benzimidazole derivatives containing 1,3,4-thiadiazole moiety, Orient. J. Chem. 33 (2017) 3138–3143. doi:10.13005/ojc/330656.

[6] Y. He, J. Yang, B. Wu, L. Risen, E.E. Swayze, Synthesis and biological evaluations

of novel benzimidazoles as potential antibacterial agents, Bioorg. Med. Chem. Lett. 14 (2004) 1217–1220. doi:10.1016/j.bmcl.2003.12.051.

[7] S. Sharma, S. Gangal, A. Rauf, Convenient one-pot synthesis of novel 2-substituted benzimidazoles, tetrahydrobenzimidazoles and imidazoles and evaluation of their in vitro antibacterial and antifungal activities, Eur. J. Med. Chem. 44 (2009) 1751–1757. doi:10.1016/j.ejmech.2008.03.026.

[8] R. Sathyanarayana, B. Poojary, R.B. Chandrashekarappa, H. Kumar, V.K. Merugumolu, Novel [1,2,4]triazolo[3,4-b][1,3,4]thiadiazine derivatives embedded with benzimidazole moiety as potent antioxidants, J. Chinese Chem. Soc. (2020) 1–16. doi:10.1002/jccs.201900452.

[9] A. Özdemir, S. Turanli, B. Çaliskan, M. Arka, E. Banoglu, Evaluation of cytotoxic activity of new benzimidazole-piperazine hybrids against human mcf-7 and a549 cancer cells, Pharm. Chem. J. 53 (2020) 1036–1046. doi:10.1007/s11094-020-02119-9.

[10] D. Ashok, M.R. Reddy, N. Nagaraju, R. Dharavath, K. Ramakrishna, S. Gundu, P. Shravani, M. Sarasija, Microwave-assisted synthesis and in vitro antiproliferative activity of some novel 1,2,3-triazole-based pyrazole aldehydes and their benzimidazole derivatives, Med. Chem. Res. 29 (2020) 699–706. doi:10.1007/s00044-020-02515-6.

[11] N.K. Rasal, R.B. Sonawane, S. V Jagtap, Potential 2,4-dimethyl-1H-pyrrole-3-carboxamide bearing benzimidazole template: Design, synthesis, in vitro

anticancer and in silico ADME study, Bioorg. Chem. 97 (2020) 103660. doi:10.1016/j.bioorg.2020.103660.

[12] Salahuddin, M. Shaharyar, A. Mazumder, Benzimidazoles : A biologically active compounds, Arab. J. Chem. 10 (2017) S157–S173. doi:10.1016/j.arabjc.2012.07.017.

[13] H. Kırpık, M. Kose, Mn(II) and Zn(II) complexes of a benzimidazole ligand having undecyl chains: Crystal structures, photophysical and thermal properties, Appl. Organomet. Chem. 33 (2019) 1–10. doi:10.1002/aoc.5224.

[14] S. Keni, A. Pingle, R. Bhogate, Benzimidazole: a propitious scaffold with multifarious theraapeutic potential, Eur. J. Biomed. Pharm. Sci. 5 (2018) 483–488.

[15] I. Castillo, B.N. Sánchez-Eguía, P.R. Martínez-Alanis, V.M. Ugalde-Saldívar, M. Flores-Alamo, Synthesis, spectroscopic, and structural characterization of mixed thioether-benzimidazole copper complexes, Polyhedron. 85 (2015) 824–829. doi:10.1016/j.poly.2014.10.022.

[16] S. Jana, R. Naskar, C.K. Manna, T.K. Mondal, Synthesis, characterization, X-ray structure and DNA binding study of palladium(II) complex with new thioether containing ONS donor ligand, J. Chem. Sci. 132 (2020) 64–73. doi:10.1007/s12039-020-01763-8.

[17] Y. Kim, J. Lee, Y. Son, S. Choi, M. Alam, S. Park, Novel nickel(II), palladium(II), and platinum(II) complexes having a pyrrolyl-iminophosphine (PNN) pincer:

Synthesis, crystal structures, and cytotoxic activity, J. Inorg. Biochem. 205 (2020) 111015. doi:10.1016/j.jinorgbio.2020.111015.

[18] M. Suwalskya, I. Castillo, B.N. Sánchez-Eguía, M.J. Gallardo, N. Dukesd, E. Santiago-Osorio, I. Aguiñiga, A.R. Rivera-Martínez, In vitro effects of benzimidazole/thioether-copper complexes with antitumor activity on human erythrocytes, J. Inorg. Biochem. 178 (2018) 87–93. doi:10.1016/j.jinorgbio.2017.10.009.

[19] B. Ay, O. Şahin, B.S. Demir, Y. Saygideğer, J.M.L.-L. Fernández, G. Mahmoudi, D.A. Safin, Antitumor effects of novel nickel-hydrazone complexes in lung cancer cells, New J. Chem. (2020). doi:10.1039/D0NJ00921K.

[20] M.J. Maroney, Nickel Bioinorganic Systems, Elsevier Ltd., 2013. doi:10.1016/B978-0-08-097774-4.00319-3.

[21] Y. Shimazaki, O. Yamauchi, Group-10 metal complexes of biological molecules and related ligands: Structural and functional properties, Chem. Biodivers. 9 (2012) 1635–1658. doi:10.1002/cbdv.201100446.

[22] A.S. Abu-Surrah, M. Kettunen, Platinum group antitumor chemistry: Design and development of new anticancer drugs complementary to cisplatin, Curr. Med. Chem. 13 (2006) 1337–1357. doi:10.2174/092986706776872970.

[23] G.A. Bain, J.F. Berry, Diamagnetic Corrections and Pascal's Constants, J. Chem. Educ. 85 (2008) 1–5. doi:10.1021/ed085p532.

[24] R.R. Gene, C.A. Koval, G.C. Lisensky, Ferrocene as an internal standard for electrochemical measurements, Inorg. Chem. (1980) 2855–2857. doi:10.1021/ic50211a080.

[25] I. Castillo, V.M. Ugalde-Saldívar, L.A. Rodríguez Solano, B.N. Sánchez Eguía, E. Zeglio, E. Nordlander, Structural, spectroscopic, and electrochemical properties of tri- and tetradentate N_3 and N_3S copper complexes with mixed benzimidazole/thioether donors, Dalton Trans. 41 (2012) 9394–9404. doi:10.1039/c2dt30756a.

[26] SAINT and SADABS; Bruker AXS Inc.: Madison, WI, 2007., (n.d.).

[27] G.M. Sheldrick, Research papers SHELXT – SHELXT – Integrated space-group and crystal- structure determination, Acta Crystallogr. Sect. A. 71 (2015) 3–8. doi:10.1107/S2053273314026370.

[28] G.M. Sheldrick, Crystal structure refinement with SHELXL, Acta Crystallogr. Sect. C. 71 (2015) 3–8. doi:10.1107/S2053229614024218.

[29] C.B. Hubschle, G.M. Sheldrick, B. Dittrich, ShelXle: a Qt graphical user interface for SHELXL, J. Appl. Crystallogr. 44 (2011) 1281–1284. doi:10.1107/S0021889811043202.

[30] CrysAlisPro, version 1.171.36.32; Oxford Diffraction Ltd.: Abingdon, U.K., 2013., (n.d.).

[31] R.C. Clark, The analytical calculation of absorption in multifaceted crystals, Acta

Crystallogr. Sect. A. 51 (1995) 8887–897. doi:10.1107/S0108767395007367.

[32] L.J. Farrugia, WinGX and ORTEP for Windows: an update, J. Appl. Crystallogr. 45 (2012) 849–854. doi:10.1107/S0021889812029111.

[33] L.A. Rodríguez Solano, I. Aguiñiga, M. López Ortiz, R. Tiburcio, A. Luviano, I. Regla, E. Santiago-Osorio, V.M. Ugalde-Saldívar, R.A. Toscano, I. Castillo, Bis(2-methylbenzimidazolyl)amine-derived copper complexes and their antineoplastic activity, Eur. J. Inorg. Chem. (2011) 3454–3460. doi:10.1002/ejic.201100301.

[34] R.N. Patel, K.K. Shukla, A. Singh, M. Choudhary, D.K. Patel, C. Cartuja, Spectral, structural, and superoxide dismutase activity of some octahedral nickel(II) complexes with tri-tetradentate ligands, J. Coord. Chem. 63 (2010) 3648–3661. doi:10.1080/00958972.2010.515985.

[35] S. Perontsis, A. Tialiou, A.G. Hatzidimitriou, A.N. Papadopoulos, G. Psomas, Nickel(II)-indomethacin mixed-ligand complexes: Synthesis, characterization, antioxidant activity and interaction with DNA and albumins, Polyhedron. 138 (2017) 258–269. doi:10.1016/j.poly.2017.09.008.

[36] S. Perontsis, A.G. Hatzidimitriou, A.N. Papadopoulos, G. Psomas, Nickel-diflunisal complexes: synthesis, characterization, in vitro antioxidant activity and interaction with DNA and albumins, J. Inorg. Biochem. 162 (2016) 9–21. doi:10.1016/j.jinorgbio.2016.06.003.

[37] U. Bossek, D. Nuhlen, E. Bill, T. Glaser, C. Krebs, T. Weyhermuller, K. Wieghardt, M. Lengen, A.X. Trautwein, Exchange coupling in an isostructurals Series of Face-

Sharing bioctahedral Complexes $[LM^{II}(\mu\text{-}X)_3M^{II}L]BPh_4$ (M= Mn, Fe, Co, Ni, Zn; X=Cl, Br; L= 1,4,7-Trimethyl-1,4,7-triazacyclononane), Inorg. Chem. 36 (1997) 2834–2843. doi:10.1021/ic970119h.

[38] W. Lee, H. Tseng, T. Kuo, Ligand-controlled nuclearity in nickel bis(benzimidazolyl) complexes, Dalton Trans. (2007) 2563–2570. doi:10.1039/b701367a.

[39] A. Mondragón, M. Flores-Alamo, P.R. Martinez, G. Aullon, V.M. Ugalde-Saldívar, I. Castillo, Electrocatalytic proton reduction by dimeric nickel complex of a sterically demanding pincer-type NS_2 aminobis(thiophenolate) Ligand, Inorg. Chem. 54 (2014) 619–627. doi:10.1021/ic502547y.

[40] P. Pirovano, B. Twamley, A.R. Mcdonald, Modulation of nickel pyridinedicarboxamidate complexes to explore the properties of high-valent oxidants, Chem. Eur. J. 24 (2018) 5238–5245. doi:10.1002/chem.201704618.

[41] P.H.A. Kankanamalage, D.M. Ekanayake, N. Singh, A.C.P. De Morais, S. Mazumder, N. Verani, A. Mukherjee, M. Lanznaster, Effect of ligand substituents on nickel and copper [N4] complexes: electronic and redox behavior, and reactivity towards protons, New J. Chem. 43 (2019) 12795–12803. doi:10.1039/c9nj01283d.

[42] M. Garai, D. Dey, H. Ram, A. Roy, N. Kole, B. Biswas, Catalytic aspects of a nickel(II)– bipyridine complex towards phosphatase and catechol dioxygenase activity, Polyhedron. 129 (2017) 114–122. doi:10.1016/j.poly.2017.03.038.

[43] D. Hong, Y. Tsukakoshi, H. Kotani, T. Ishizuka, K. Ohkubo, Y. Shiota, K. Yoshizawa, S. Fukuzumi, T. Kojima, Mechanistic insights into homogeneous electrocatalytic and photocatalytic hydrogen evolution catalyzed by high-spin Ni(II) complexes with S_2N_2-type tetradentate Ligands, Inorg. Chem. 57 (2018) 7180–7190. doi:10.1021/acs.inorgchem.8b00881.

[44] I. Castillo, M. Suwalsky, M.J. Gallardo, V. Troncoso, B.N. Sánchez-Eguía, E. Santiago-Osorio, I. Aguiñiga, A.K. González-Ugarte, Structural and functional effects of benzimidazole/thioether-copper complexes with antitumor activity on cell membranes and molecular models, J. Inorg. Biochem. 156 (2016) 98–104. doi:10.1016/j.jinorgbio.2015.12.022.

[45] D. Rocco, L.K. Batchelor, G. Agonigi, S. Braccini, F. Chiellini, S. Schoch, T. Biver, T. Funaioli, S. Zacchini, L. Biancalana, M. Ruggeri, G. Pampaloni, P.J. Dyson, F. Marchetti, Anticancer potential of diiron vinyliminium complexes, Chem. Eur. J. (2019) 14801–14816. doi:10.1002/chem.201902885.

[46] A.S. Estrada-montaño, A.D. Ryabov, A. Gries, C. Gaiddon, R. Le Lagadec, Iron (III) pincer complexes as a strategy for anticancer studies, Eur. J. Inorg. Chem. (2017) 1673–1678. doi:10.1002/ejic.201601350.

[47] M. Liu, X. Song, Y. Wu, J. Qian, J. Xu, Cu(II)-TACN complexes selectively induce antitumor activity in HepG-2 cells via DNA damage and mitochondrial-ROS-mediated apoptosis, Dalton Trans. 49 (2020) 114–123. doi:10.1039/c9dt03641e.

Declaration of interests

☒ The authors declare that they have no known competing financial interests or personal relationships that could have appeared to influence the work reported in this paper.

☐The authors declare the following financial interests/personal relationships which may be considered as potential competing interests:

Graphical abstract

Bis(benzimidazole)thio- and selenoether ligands afford mono- and bimetallic Ni(II) complexes in the solid state, with monometallic behavior in solution. They show moderate cytotoxic activity towards cancer cell lines, in some cases with better selectivity than a Cu(II) analog.

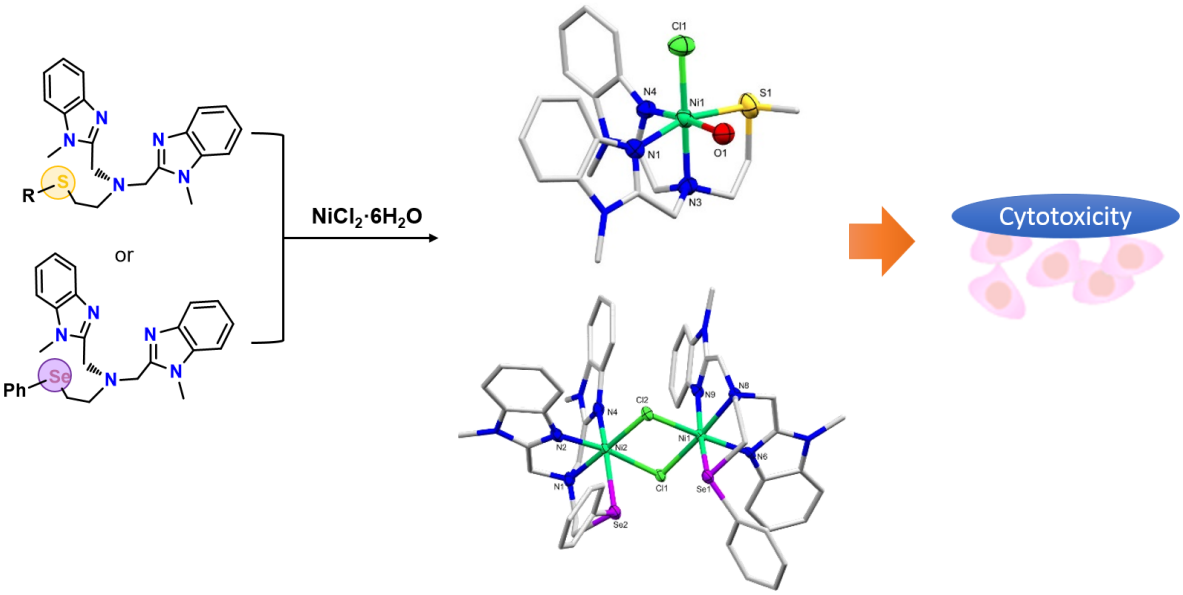

Highlights

- Synthesis of 4 Ni(II) complexes with bis(benzimidazole)thio/selenoether ligands.
- All Ni(II) complexes were characterized by X-ray crystallography.
- Mass spectrometry confirms in all cases monomeric species in solution.
- *In vitro* cytotoxicity of the complexes against cancer cell lines was studied.
- One Ni(II) complex exhibits greater selectivity than its Cu(II)-based analog.